Polymer 50 (2009) 42–49

Contents lists available at ScienceDirect

Polymer

journal homepage: www.elsevier.com/locate/polymer

Rheological properties of RAFT-mediated poly(styrene-*co*-butyl acrylate)–clay nanocomposites [P(S-*co*-BA)-PCNs]: Emphasis on the effect of structural parameters on thermo-mechanical and melt flow behaviors

Austin Samakande, Ronald D. Sanderson, Patrice C. Hartmann*

UNESCO Associated Centre for Macromolecules, Department of Chemistry and Polymer Science, University of Stellenbosch, Private Bag X1, 7602 Matieland, South Africa

ARTICLE INFO

Article history:
Received 8 July 2008
Received in revised form
12 October 2008
Accepted 28 October 2008
Available online 7 November 2008

Keywords:
Polymer–clay nanocomposite
Reversible addition–fragmentation chain transfer
Miniemulsion

ABSTRACT

RAFT-mediated random poly(styrene-*co*-butyl acrylate)-[*N*-(4-((((dodecylthio)-carbonothioyl)thio)-methyl)benzyl)-*N*,*N*-dimethylethanammonium]–clay nanocomposites (P(S-*co*-BA)–DCTBAB–PCNs) and poly(styrene-*co*-butyl acrylate)-[*N*,*N*-dimethyl-*N*-(4-(((phenylcarbonothioyl)thio)-methyl)benzyl)ethanammonium]–clay nanocomposites (P(S-*co*-BA)–PCDBAB-PCNs) were prepared by miniemulsion free-radical polymerization. The RAFT agents (i.e. DCTBAB and PCDBAB) were anchored onto the clay layers prior to polymerization, and were able to control the polymerization process, as evident from the decreasing molar mass and polydispersity index (PDI) values as the concentration of the RAFT agent in the system increased. The efficiency of the anchored RAFT agents increased as the RAFT agent concentration in the system increased, i.e. as the clay loading increased. The nanocomposites that were prepared were found to have a partially exfoliated morphology at low clay loadings, as determined by SAXS and TEM, whereas, at high clay loadings the morphology changed to become predominantly intercalated. The thermo-mechanical properties of the nanocomposites were found to be a function of the molar mass, PDI, PCN morphology, and clay loading. In the glassy state, the storage modulus was seen to effectively decrease as clay loading increased, whereas the opposite was true for the loss modulus and tan delta. At low clay loadings the melt rheological properties were dominated by the matrix effects, whereas at high clay loadings the effect of the clay filler dominated, resulting in pseudo solid–liquid-like behavior.

1. Introduction

The discovery of the nylon 6 polymer–clay nanocomposite (nylon 6-PCN) by the Toyota research group in the early 1990s marked the dawn of a new era in the field of polymer–clay nanocomposites [1]. The nylon 6-PCN that they prepared had better thermal and mechanical properties than neat nylon 6 polymer, which resulted in its use in the automotive industry. Toyota's landmark discovery has subsequently led to concerted efforts in research and development towards various aspects of PCNs from their synthesis to their applications. A vast amount of literature on PCNs has appeared over only a decade. Most of the articles to date have focused on uncontrolled radical polymerization systems [2–4]. However, as knowledge of controlled radical polymerization systems are increasing by the day [5,6]. PCNs that have been synthesized using controlled radical polymerization (CRP) have started to appear [7–11]. Of all the CRP techniques the RAFT technique is believed to be more robust and versatile [6].

There are few articles that have focused on RAFT-mediated PCNs synthesis and characterization [12–19]. As such, our group has recently focused on RAFT-mediated PCNs synthesis and characterization. To date we have synthesized novel RAFT agents that can be attached to clay [20]. We have shown the effectiveness of these RAFT agents on the control of polymerization in bulk and miniemulsion during PCNs synthesis [21,22]. Moreover, we have investigated the thermo-mechanical properties of the resultant PCNs. However, no characterization of the melt rheological properties of RAFT-mediated PCNs has been reported.

Polymer melt rheological studies provide information that is similar to that of DMA but, importantly, they also provide more valuable information pertaining to the behavior of a polymer under processing conditions prior to the formation of the final product. The melt rheological properties of PCNs are dependent on their molar mass, polydispersity index (PDI), clay loading and the PCN morphology [23–29]. The complex viscosity of PCNs has been shown to be typically non Newtonian in behavior, as a result of the nanodispersion of the clay platelets [23,29]. The storage and loss

* Corresponding author. Tel.: +27 21 808 3176; fax: +27 21 808 4967.
E-mail address: hartmann@sun.ac.za (P.C. Hartmann).

0032-3861/$ – see front matter © 2008 Elsevier Ltd. All rights reserved.
doi:10.1016/j.polymer.2008.10.050

moduli have been reported to show non-terminal solid-like behavior at low frequencies due to the presence of the clay platelets [25,26,28–33], while in the high frequency region monotonic increases in G^{I} and G^{II} are observed as clay loading increases [25,26,28,30,34]. However, most of the PCNs that have been prepared and characterized to date have been synthesized by uncontrolled radical polymerization. This implies that; various explanations they provided for the physical and chemical properties of the PCNs they investigated did not fully take into account the effects of molar mass, polydispersity index and the changing PCN morphology.

This contribution reports on the preparation of poly(styrene-*co*-butyl acrylate)-[*N*-(4-((((dodecylthio)carbonothioyl)thio)methyl) benzyl)-*N*,*N*-dimethylethanammonium]-clay nanocomposites (P(S-*co*-BA)–DCTBAB–PCNs) and poly(styrene-*co*-butyl acrylate)-[*N*,*N*-dimethyl-*N*-(4-(((phenylcarbonothioyl)thio)methyl)benzyl) ethanammonium]-clay nanocomposites (P(S-*co*-BA)–PCDBAB-PCNs) by RAFT-mediated free-radical polymerization. A discussion of the impact of molar mass, PCN morphology and clay loading have on thermo-mechanical and melt flow properties is given.

2. Materials and methods

2.1. Chemicals

Styrene (99%, Aldrich) was purified by washing with 0.3 M KOH, followed by distillation at 40 °C under reduced pressure. Sodium dodecyl sulphate (SDS) (99%, Aldrich) and hexadecane (99%, Aldrich) were used as-received. Azobisisobutyronitrile (AIBN, Aldrich) was purified by recrystallization from methanol. Sodium Montmorillonite (Na-MMT) was obtained from Southern Clay Products (Texas, USA). Deionized water was obtained from a Millipore Milli-Q-purification water system. *N*,*N*-dimethyl-*N*-(4-(((phenylcarbonothioyl)thio)methyl)benzyl)ethanammonium bromide (PCDBAB), *N*-(4-((((dodecylthio)carbonothioyl)thio)methyl) -benzyl)-*N*,*N*-dimethylethanammonium bromide (DCTBAB), PCDBAB-MMT and DCTBAB-MMT, (i.e. RAFT-MMT) clays were prepared as described by us in previous papers [20,21]. The chemical structures of the RAFT agents PCDBAB and DCTBAB are shown in Scheme 1.

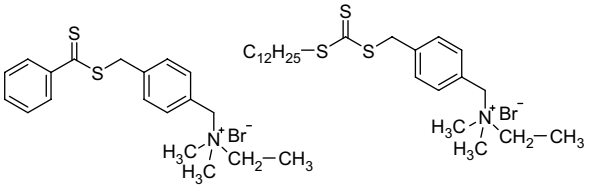

Scheme 1. Structures of PCDBAB (left) and DCTBAB (right) RAFT agents, respectively.

2.2. Typical preparation of PS-co-BA PCNs using RAFT-mediated free-radical miniemulsion polymerization

Predetermined quantities of RAFT-MMT, AIBN, a styrene and n-butyl acrylate mixture (50:50 by mass) and hexadecane (oil phase) (c.f. Table 1) were stirred together overnight in a three-necked round-bottomed flask, to allow effective swelling of the clay galleries by the monomer.

To the oil phase, SDS solution (water phase) was added and the resulting biphasic mixture was stirred for a further 30 min to obtain a pre-emulsion. The pre-emulsion was then sonicated for 30 min using a Sonics Vibra Cell Autotune series 750VCX high intensity ultrasonic processor, in a water jacketed vessel. The amplitude was set at 90%, and the temperature cut off for the probe was set at 40 °C. The average energy expended was ~180 kJ. The resultant miniemulsion was then immersed in an oil bath. The three necks of the round-bottomed flask were fitted with a condenser (main neck), a nitrogen gas inlet and a septum (side necks). The miniemulsion sample was then purged with nitrogen for 30 min before the temperature was rapidly increased to 75 °C to start the polymerization. The polymerization was carried out for 6 h at 75 °C.

Table 1
Initial quantities of reagents in the miniemulsions.

Polymer	RAFT (g)	MC (g)	S (g)	BA (g)	AIBN (g)	SDS (g)	HD (g)
PS-D-St	0.080	–	3.543	3.506	0.016	0.174	0.357
PS-D-1		0.100	4.910	4.914	0.009	0.248	0.487
PS-D-2		0.198	4.914	4.900	0.012	0.248	0.499
PS-D-3		0.356	4.917	4.917	0.027	0.248	0.503
PS-D-5		0.497	4.900	4.906	0.030	0.248	0.492
PS-P-St	0.075	–	3.515	3.537	0.018	0.115	0.350
PS-P-1		0.101	4.909	4.908	0.010	0.164	0.508
PS-P-2		0.198	4.892	5.030	0.014	0.164	0.509
PS-P-3		0.356	4.923	4.909	0.023	0.164	0.489
PS-P-5		0.490	4.900	4.899	0.024	0.164	0.488

Key: MC = modified clay, S = styrene monomer, BA = butyl acrylate monomer, SDS = sodium dodecyl sulphate and HD = hexadecane.

A similar procedure was used for the synthesis of clay-free RAFT-mediated styrene-*co*-butyl acrylate miniemulsion polymerization, the only difference now being that the oil and the water phases were mixed after being stirred separately for 1 h.

2.3. Analyses

Size Exclusion Chromatography (SEC) was carried out using a Waters 600E system controller equipped with a Waters 610 fluid unit pump and a Waters 410 differential refractometer as detector. Prior to analysis samples were reverse ion-exchanged as follows. Quantities of P(S-*co*-BA)-PCN (0.2 g) and LiCl (0.06 g) were dissolved in THF (10 ml) and refluxed at 70 °C for 3 h. The solution was filtered through Celite, and the polymer was precipitated from methanol and dried. GPC analysis, using THF as mobile phase and an initial polymer concentration of 5 mg/mL, was performed on clay-free polymer solutions. Dynamic light scattering (DLS) measurement of the polymer in THF solution showed no peak/s characteristic of clay particles, thus indicating that the chains were completely detached from the clay particles before SEC analysis.

Small angle X-ray scattering (SAXS) measurements were performed in a transmission configuration at 298 °K. A copper rotating anode X-ray source (functioning at 4 kW), with a multilayer focusing Osmic monochromator giving high flux (10^8 photons/sec) and punctual collimation, was used. An image plate 2D detector was used. Diffraction patterns were obtained, giving diffracted intensity as a function of the wave vector q. The calculation of the q values is described elsewhere [35].

Transmission electron microscopy (TEM) was used to directly visualize the morphology of the clay particles in polystyrene-clay nanocomposites at the nanometer level. Bright field TEM images were recorded using a LEO 912 transmission electron microscope, at an accelerating voltage of 120 kV. Prior to analysis the P(S-*co*-BA)-PCNs miniemulsion samples were dried into thin films, embedded in epoxy resin and cured for 24 h at 60 °C. The embedded films were then ultra-microtomed with a diamond knife on a Reichert Ultracut S ultra microtome at room temperature. This resulted in sections with a nominal thickness of ~100 nm. The sections were transferred from water at room temperature to 300-mesh copper grids, which were then transferred to the TEM apparatus.

Dynamic mechanical analysis (DMA) and rheology. Determinations of the DMA and the rheology of the P(S-*co*-BA)-PCN films were carried out using a Physica MCR 501 apparatus (Anton Paar, Germany). For DMA measurements, parallel-plate geometry (diameter 25 mm) was used, with a 1 mm gap distance and a constant strain of 0.1%. Measurements were carried out from 90 °C to −20 °C at a heating rate of −5 °C/min, an oscillation frequency of 1 Hz, and a normal force of 5 N.

Rheology measurements were carried out at 95 °C, using an angular frequency range of 600–0.01 rad/sec. Parallel-plate geometry (diameter 25 mm), with a gap distance of 1 mm and a constant strain of 1% was used, in order to carry out measurements within the linear viscoelastic (LVE) range.

3. Results and discussion

We copolymerized styrene and n-butyl acrylate, initially using a 50:50 (by mass) monomer ratio. This ratio has already been shown to yield a random polystyrene-*co*-butyl acrylate that can form film at room temperature [33]. Moraes et al. [33] reported on the preparation of P(S-*co*-BA) in the presence of clay by miniemulsion free-radical polymerization and obtained random P(S-*co*-BA)-PCNs. It is hence believed that we also obtained a random copolymer. Moreover, Fildermann et al. [36] reported that the inclusion of RAFT does not significantly change the copolymer composition and the respective reactivity ratios of the comonomers.

The molar masses and the PDI values of the copolymers we synthesized decreased as the clay loading increased, as expected in RAFT-mediated polymerization systems (see Table 2).

The experimental molar masses were higher than the theoretically calculated ones in all cases. This is attributed to the fact that the anchored RAFT agents do not act as very efficient transfer agents when compared to free RAFT agents (unattached) [13,21]. On the other hand, the PDI values of the random copolymers were comparable to those found in literature for RAFT-mediated copolymers [38,39]. The decrease in conversion with increased clay loading is mainly attributed to the presence of the RAFT agents on the clay surfaces that retards the polymerization progress [21]. An increase in RAFT agent at the same monomer concentration leads to the exacerbation of the decrease in the polymerization progress as is observed here. The extent of the retardation was more pronounced for dithiobenzoate (PCDBAB) than for trithiocarbonate (DCTBAB) mediated systems in accordance with literature [40,41].

3.1. Morphology of polymer–clay nanocomposites

The SAXS patterns of P(S-*co*-BA)-PCNs are shown in Fig. 1. The peak of particular interest is the broad peak at the *q* value of 4.14. This peak at low clay loadings is very broad and of very low intensity, indicating a partially exfoliated structure. At higher clay loadings (P(S-*co*-BA)-D-5% and P(S-*co*-BA)-P-5%) the peak is well defined and intense, indicating an intercalated morphology. The change in the nanocomposite morphology is ascribed to a decreasing molar mass. As the polymer chains grow they exert pressure on the clay platelets, causing them to move apart, which results in an exfoliated structure [42]. However, in our case, as the clay loading is increased there is a reduction in the effective molar mass of the chains. This results in intercalated morphology at high clay loading and, concomitantly, lower molar mass polymer chains relative to low clay loadings.

Surprisingly, two groups of relatively sharp peaks were seen in the P(S-*co*-BA)-PCNs as well as from the neat P(S-*co*-BA) blank sample, (i.e. P(S-*co*-BA) standard) with *q* values and the respective *d* spacing in brackets: (*) [1.64 (3.83 nm), 3.27 (1.92 nm); 4.90 (1.28 nm)] and (⊗) [1.99 (3.16 nm), 3.97 (1.58 nm); 5.98 (1.05 nm)]. In each group of peaks the absolute *d* spacing values follow the pattern 1:½:1/3, typical of a lamellar structure. These lamellar structures are believed to be due to the self assembly of hexadecane and SDS in the presence of P(S-*co*-BA). It is believed that the self assembly of hexadecane and SDS occur during film formation of the PCNs. The self assembly behavior of SDS and hexadecane in literature show that they can both form lamellar structures [43–46]. However, and even more surprisingly, the presence of the clay layers seems to be hindering this self assembly. Moreover, it is worth mentioning that the clay loading seems to affect the self assembly of hexadecane and SDS in an opposite way, depending on the RAFT agent used for surface modification prior polymerization. Reasons for this behavior are still unclear, although it is likely to be due to the difference in the chemical structure of the Z group of the RAFT agents used. After the polymerization mediated by DCTBAB, the presence of dodecyl alkyl groups at the end of the PS chains may promote compatibility between the polystyrene matrix and hexadecane. This effect cannot take place when the polymerization is mediated by PCDBAB which bears a phenyl Z group.

The TEM images of dried samples (films) of P(S-*co*-BA)–DCTBAB-1% and P(S-*co*-BA)–PCDBAB-1% (c.f. Fig. 2) showed predominantly a partially exfoliated structure, with a typical dispersion in the polymer matrix of both individual clay platelets and stacks of few intercalated ones. This is in accordance with what was observed by SAXS.

3.2. Mechanical properties

The three main parameters of DMA measurements are (i) the storage modulus (G^{I}), which is a measure of elastic response to the deformation; (ii) the loss modulus (G^{II}), which is a measure of

Table 2
Molar masses, polydispersity indices and percentage conversions for various P(S-*co*-BA)-PCNs prepared.

Polymer	Calc MC_g/M_g%	Exp MC_g/P_g%	$[M]_0/[R]_0$	Calc M_n (kg/mol)	Exp M_n (kg/mol)	PDI	Conv (%)
PS-*co*-BA St	–	–	–	–	235.8	3.8	86.7
PS-*co*-BA P-St	–	–	331.6	9.9	12.2	1.3	23.8
PS-*co*-BA-P-1%	1.0	1.1	1 133.4	101.8	114.2	2.0	87.7
PS-*co*-BA-P-2%	2.0	2.2	537.2	53.5	73.5	1.9	86.7
PS-*co*-BA-P-3.6%	3.6	4.6	351.4	24.3	42.2	1.7	70.0
PS-*co*-BA-P-5%	5.0	6.9	233.2	15.5	28.3	1.7	60.3
PS-*co*-BA-D-St	–	–	406.9	26.4	35.7	2.3	71.1
PS-*co*-BA-D-1%	1.0	1.1	1 249.7	114.8	191.8	2.4	91.2
PS-*co*-BA-D-2%	2.0	2.2	630.5	61.2	91.3	2.5	89.8
PS-*co*-BA-D-3.6%	3.6	4.0	322.0	31.3	49.1	2.2	86.5
PS-*co*-BA-D-5%	5.1	5.6	251.0	23.4	36.8	2.2	85.0

Key: Calc MC_g/M_g% calculated mass ratio of modified clay to monomer, *Exp* MC_g/P_g% Experimental mass ratio of modified clay to polymer; $[M]_0/[R]_0$ initial molar ratio of monomer to RAFT, *Calc* M_n = theoretical molar mass calculated using the equation $M_n = ([M]_0 M_S x)/([RAFT]_0) + M_{RAFT}$ [37], where $[M]_0$ = initial monomer concentration, M_S = molar mass of monomer, x = conversion, M_{RAFT} = molar mass of RAFT, $[RAFT]_0$ = initial concentration of RAFT; *Exp* M_n = experimental molecular mass; *PDI* = polydispersity indices of the polymer obtained, as determined by SEC. P(S-*co*-BA)-P and P(S-*co*-BA)-D refer to PCNs based on PCDBAB and DCTBAB, respectively.

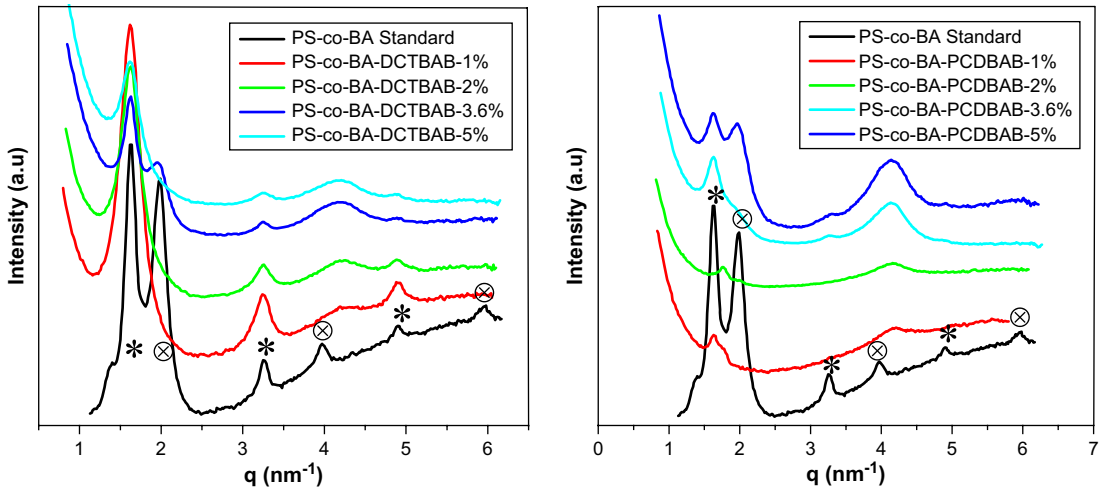

Fig. 1. SAXS patterns of P(S-*co*-BA)-PCNs.

the plastic response, and (iii) tan δ, i.e. the ratio of G^{II}/G^{I}. Tan δ is used to determine molecular mobility. The interactions taking place at the interface between the polymer matrix and clay's silicate layers decrease the macromolecule's mobility in the polymer segments near the interface [47], which leads to improved mechanical properties. In general, G^{I} values increase with an increase in clay loading for nanocomposites below the glass transition temperature (T_g) (i.e. in the glassy state). The same effect occurs in the rubbery region [27,48–50]. This is attributed to the large aspect ratio of the structural hierarchy on the nanoscale level. Nanocomposites with exfoliated morphologies have been shown to have exceptionally enhanced thermo-mechanical properties relative to the intercalated and the conventional microcomposites. When nanoclay is present in a PCN sample the G^{II} and tan δ peaks have been shown to broaden and shift to higher temperatures. This has been attributed to restricted chain mobility [30,49,51,52], associated with an increase in the T_g of the PCN relative to the neat polymer. The broadness of the T_g peak can be attributed to an increase in the PDI of the polymer material given most of the chains will be attached and a few will be free. Moreover the distance of a polymer segment from the clay/polymer interface results in different sensitivity towards an applied force that causes movement.

The storage moduli of P(S-*co*-BA)-PCNs as a function of temperature (cf. Fig. 3), were found to be superior to that of the non-clay-containing random copolymer. However, as the clay loading increased, and concurrently the molar mass decreased, the storage modulus effectively decreased. This behavior was similar to that of RAFT-mediated PS-clay nanocomposites prepared in a similar manner [22].

Thus the effect of both molar mass and PCN morphology seems to have a dominant effect on G^{I}. It was expected that an increase in clay loading would result in an increase in the storage modulus. The recorded storage moduli of the P(S-*co*-BA)-PCN films also showed interesting effects of the molar mass and clay loading effects in the profiles of the variation of G^{I} against temperature curves. The width of the rubbery plateau (i.e. at temperatures embraced above the transition from the glassy state and below the final transition into the viscous liquid state) is indicative of the molar mass of the polymer [28,53]. It is seen that the width of the rubbery plateau becomes narrower with increasing clay loading, further confirming our deductions that the molar mass decreases with increasing clay loading. This is also an indication that the RAFT agents within the clay galleries effectively controlled the polymerization process. Moreover, the extent (drop) of the transition from the glassy state to the rubbery region decreases with increasing clay loading, further proving that the clay layers are indeed acting in a similar way as crosslinkers towards the polymer chains. The presence of crosslinkers in a polymer sample is known to decrease the length of the transition from the glassy state to the rubbery region [28,53].

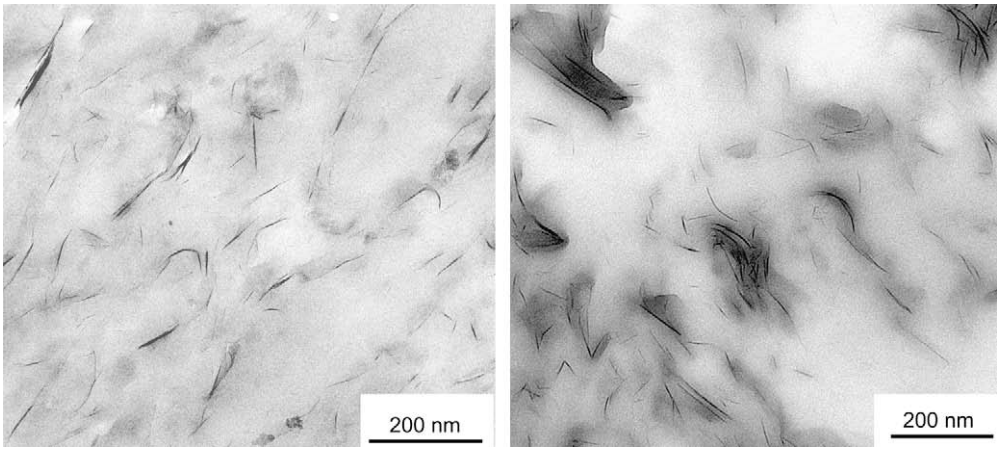

Fig. 2. TEM images of P(S-*co*-BA)–DCTBAB-1% (left) and P(S-*co*-BA)–PCDBAB-1% (right).

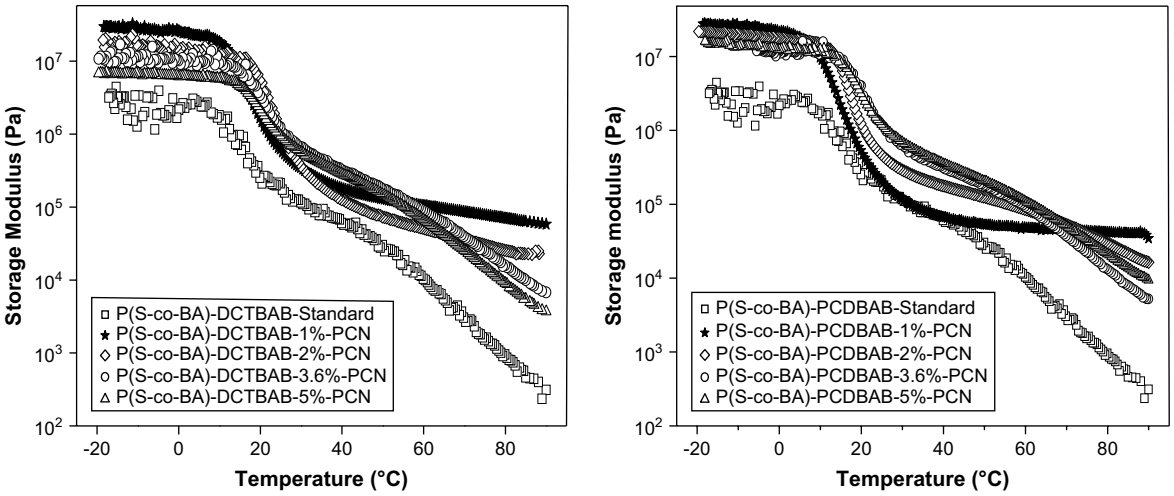

Fig. 3. Storage modulus as a function of temperature of P(S-*co*-BA)–DCTBAB–PCNs (left) and P(S-*co*-BA)–PCDBAB-PCNs (right).

The loss moduli peaks of the P(S-*co*-BA)-PCNs as a function of temperature shifted to higher temperature, relative to the standard neat copolymers, indicating an increase in T_g. This is a direct result of the incorporation of clay layers that act as crosslinkers in the polymer network. However, as the clay loading increased the peak maximum did not shift significantly further to higher temperatures (see Fig. 4).

These results indicate that the T_g of the P(S-*co*-BA)-PCNs did not significantly change as the clay loading increased and, simultaneously, the molar mass decreased. These results are indicative of a balance of effects of the clay loading and the molar mass. Our results are in agreement with those of Moraes et al. [33] who prepared the same P(S-*co*-BA)-PCNs using miniemulsion polymerization, although their nanocomposites were prepared using an uncontrolled free-radical polymerization method.

The tan delta peaks of the P(S-*co*-BA)-PCNs were also shifted to higher temperature relative to the neat P(S-*co*-BA) standard (see Fig. 5). The molar mass and clay loading effects were also evident in these tan delta peaks as seen by the shape of the peaks above the transition [53]. As the clay loading increased and molar mass decreased the transition peak became small and the values of tan delta after the transition peak increased monotonously. As opposed to previous reports that the tan delta peak broaden as clay loading increases, in our case the reverse is true probably due to the narrowing PDI in the PCNs as clay loading increases.

The effect of % clay loading on the relative values of tan delta seem to have an opposite effect depending on whether the temperature is below or above the T_g. In the glassy state (below T_g), the presence of clay enhances the solid-like character of the material, as tan delta gradually decreases as % clay loading increases. On the contrary, in the viscous state (above T_g), the presence of clay enhances further the liquid-like character of the material, as tan delta gradually increases with the clay loading. Although this later effect is due to a decrease of the molar mass as the clay loading increases, the resulting overall effect is of particular interest for industrial processability as an increase in clay loading seems to enhance both flow properties above T_g and toughness of the material below T_g.

3.3. Melt rheology

Melt rheological properties of the PCNs are important in the consideration of their possible processing. The complex viscosity of PCNs with various clay loading at 95 °C was plotted as a function of angular frequency for both series PCDBAB and DCTBAB (see Fig. 6). The DCTBAB and PCDBAB mediated PS-*co*-BA polymer standards

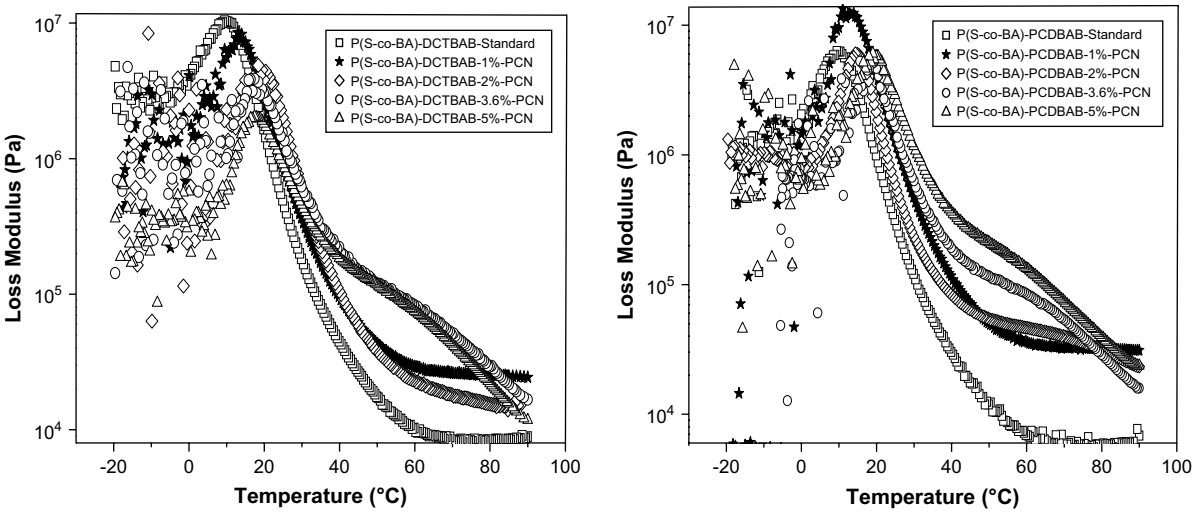

Fig. 4. Loss modulus as a function of temperature of P(S-*co*-BA)–DCTBAB–PCNs (left) and P(S-*co*-BA)–PCDBAB-PCNs (right).

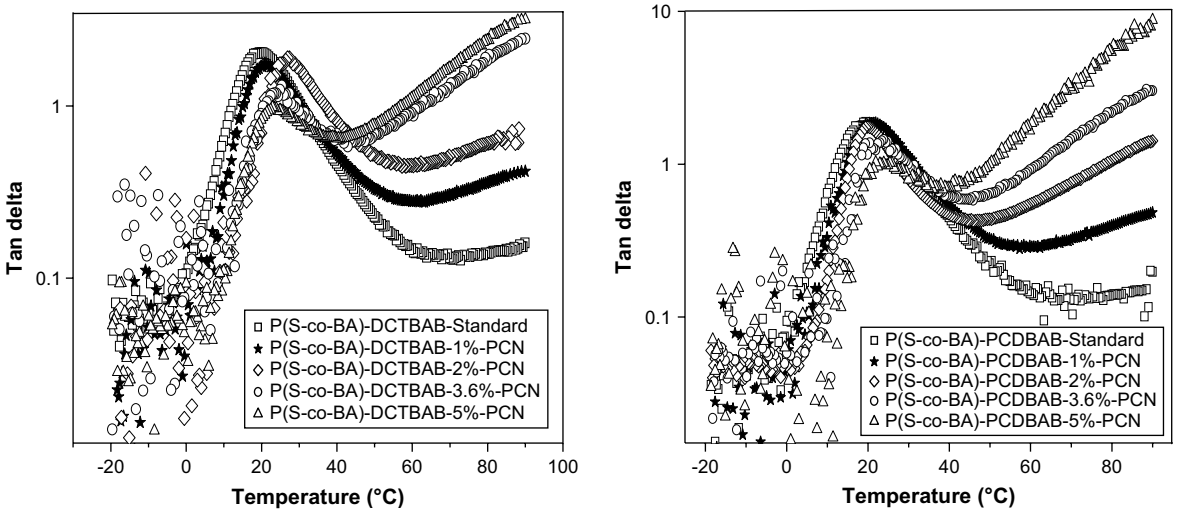

Fig. 5. Tan delta as a function of temperature for P(S-*co*-BA)-PCNs, based on DCTBAB (left) and PCDBAB (right), respectively.

without clay showed typical Newtonian behavior [26]. The complex viscosity (η^*) increased linearly with a decrease in the angular frequency up to about 10 rad/s, whereas for lower frequencies, η^* tends to become independent of the angular frequency. This is typical of unfilled polymers as reported in literature [23,29].

The complex viscosities of both P(S-*co*-BA)–DCTBAB–PCNs and P(S-*co*-BA)–PCDBAB-PCNs were dependent on a number of factors: (i) molar mass, (ii) clay loading and (iii) PCN morphology. The value of the onset of the complex viscosity (high frequency region) was found to increase monotonously with an increase in clay loading. The frequency dependence of the complex viscosity for 1% and 2% clay loadings showed typical Newtonian behavior. It was found to be dominated by the molar mass and showed little dependence on the clay loading and morphology. Here the increase in complex viscosity observed as the angular frequency decreased was more pronounced for the PCNs with 1% clay loading, and which ultimately had higher molar mass than the PCNs with 2, 3.6 and 5% clay loadings. Viscosities of the samples with 1% clay loading became independent of angular frequency for values below 0.01 rad/sec, whereas at 2% clay loading this effect was observed for angular frequencies below 0.1 rad/sec. This showed the dependency of the viscosity on molar mass and PCN morphology. At 3.6% clay loading and above, the complex viscosity curves showed a different pattern, as the complex viscosity continuously increased even at very low angular frequencies. This showed their typical non-Newtonian behavior, i.e. pseudo solid-like behavior, as reported in literature [23,29]. For frequencies above 0.3 rad/sec the melt flow properties of the nanocomposites were dominated by the molar mass, as they tend to be Newtonian in behavior, i.e. there is a tendency to be independent of clay loading by showing pseudo plateaus.

The variation of G^{I} and G^{II} of the P(S-*co*-BA) with angular frequency at 95 °C follows a similar pattern as for the complex viscosity: the onset (high frequency region) of both storage and loss moduli increases monotonously with clay loading, as reported in literature [25,26,28,30,34,54]. This clearly shows that the presence of clay increases the stiffness of the material. However, storage and loss moduli of the nanocomposites at 1% and 2% clay loadings were dominated by the molar mass of the polymer matrix as they do not show the solid–liquid character typical of PCNs (c.f. Fig. 7) [23–25,28].

Fig. 7 shows that for 1% and 2% clay contents have a plateau in the high angular frequency region, before they start to decrease. This is more pronounced for the 1% clay loading. For the 3.6 and 5% clay loadings the loss and storage moduli quickly decrease with decreasing angular frequency. These are indications of the

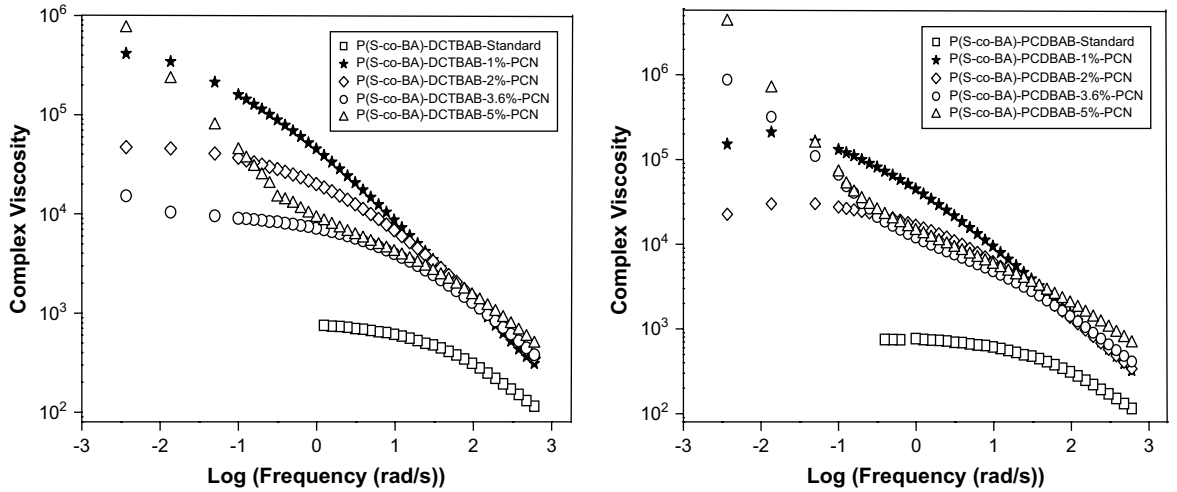

Fig. 6. Complex viscosity as a function of angular frequency for P(S-*co*-BA)–DCTBAB–PCNs (left) and P(S-*co*-BA)–PCDBAB-PCNs (right).

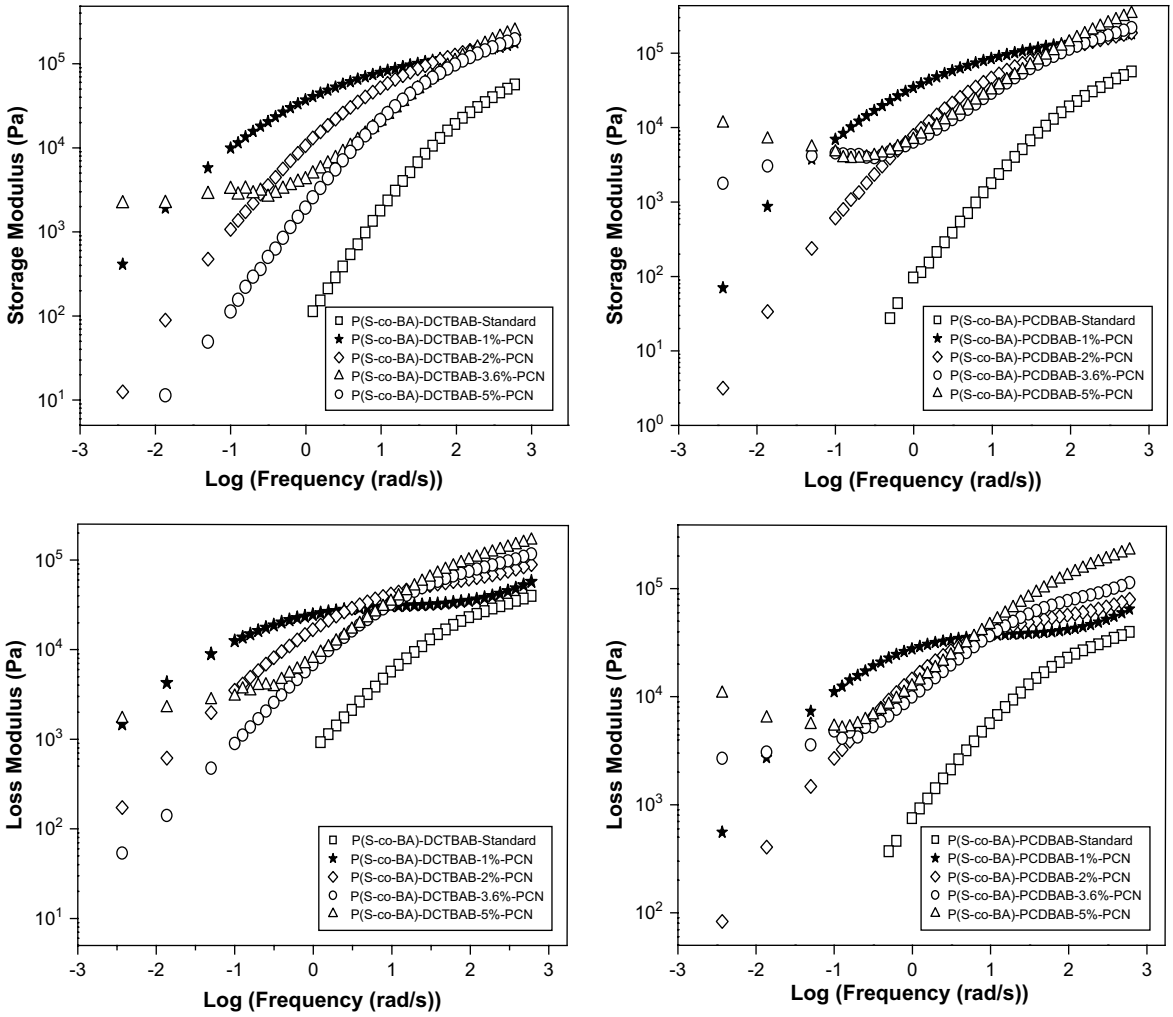

Fig. 7. Variation of storage modulus (G^{I}) and loss modulus (G^{II}) with angular frequency (ω) for (left) P(S-*co*-BA)–DCTBAB–PCNs and (right) P(S-*co*-BA)–PCDBAB-PCNs.

dependence of the rheological properties on the molar mass of the matrix [27,54]. Ma et al. [32] have reported minute differences in the storage and loss moduli of the ABS and ABS-graft-MAH PCNs in the high frequency region. This shows that in the high frequency region matrix effects are dominant. At low angular frequency PCNs with 1% and 2% clay loadings show a fast decreasing loss and storage moduli with decreasing angular frequency, which is characteristic of homopolymers without filler. This indicates that at low clay loadings the melt flow properties of PCNs were not significantly influenced by the clay loading but rather by the matrix and the polydispersity indices. At the 3.6 and 5% clay loadings for both PCNs, non-terminal pseudo solid–liquid-like behavior was observed [23–26,28,29,31–33,55]. The dependency of the storage and loss moduli on angular frequency diminishes and becomes more dependent on the clay loading [28,31]. These effects are a result of the increased frictional interactions of the clay particles, as well as the strong polymer–clay interactions [24,26]. Our results of pseudo solid–liquid-like behavior at clay loadings of greater than 3% agree well with those of Krishnamoorti et al. [28] who also observed similar effects for their clay attached (end-tethered) poly(ε-caprolactone)-clay nanocomposites, as in our case, whereas Ren et al. [14] only observed this effect at 6.7% clay loading for non-clay-attached polystyrene–polyisoprene–clay nanocomposites. The differences in the clay levels where pseudo solid–liquid-like behavior is observed can thus be attributed to whether the polymers are attached or not to the clay layers.

Another important parameter related to the melt rheology of PCNs is the crossover frequencies (i.e. frequencies at which values of storage and loss moduli are equal). These angular frequency points give an indication of the relaxation times of the polymer chains in the PCNs (see Table). The number of these crossover points also gives an indication of the arrangement of the clay platelets relative to each other, and of the number density of the clay platelets [29]. On the other hand, the terminal slope of the storage and loss moduli versus angular frequency gives an indication of the clay morphology and the polydispersity of the polymers. It is expected that at the terminal end in the low angular frequency region, $G^{I} \propto \omega^{2}$ and $G^{II} \propto \omega^{1}$ for monodisperse unfilled polymers. In essence the terminal gradient of the variation of storage modulus with angular frequency, should be theoretically equal to 2 and the terminal slope of the loss modulus equal to 1 for a homogeneous and monodisperse homopolymer [24,25,28]. Deviations from these values, (i.e. terminal gradients) may be due to polydispersity, the P(S-*co*-BA)-PCNs morphology, and/or clay loading.

G^{I} and G^{II} crossover frequencies and corresponding relaxation times are reported in Table 3. The relaxation times of all P(S-*co*-BA)-PCNs were found to be greater than that of the neat PS-*co*-BA copolymer standard, although within the same series of P(S-*co*-BA)-PCNs, the relaxation time decreases as the clay loading increases. This is surprising, as the presence of clay was expected to increase the relaxation time of the polymer chains of the matrix [31]. However, the decrease of molar mass with increasing clay

Table 3
Terminal gradients and the associated relaxation times of P(S-*co*-BA)-PCNs.

Polymer	$\Delta G^{I}/\Delta\omega$	$\Delta G^{II}/\Delta\omega$	ω_1 (rad/s)	T_1 (s)	ω_2 (rad/s)	T_2 (s)
PS-*co*-BA St	1.46	0.94	151.92	0.04	–	–
PS-*co*-BA-P-1%	1.93	1.21	0.50	12.57	–	–
PS-*co*-BA-P-2%	1.86	1.22	6.16	1.02	–	–
PS-*co*-BA-P-3.6%	0.41	0.10	24.33	0.26	0.16	39.27
PS-*co*-BA-P-5%	0.25	0.05	76.44	0.08	0.05	125.66
PS-*co*-BA-D-1%	1.38	0.82	0.25	25.13	–	–
PS-*co*-BA-D-2%	1.50	0.97	3.90	1.61	–	–
PS-*co*-BA-D-3.6%	0.73	0.93	24.33	0.26	–	–
PS-*co*-BA-D-5%	0.00	0.21	76.44	0.08	0.03	209.44

Key: $\Delta G^{I}/\Delta\omega$ = terminal gradient i.e. increase in storage modulus/increase in angular frequency; $\Delta G^{II}/\Delta\omega$ = terminal gradient i.e. increase in loss modulus/increase in angular frequency; ω_1 = first crossover angular frequency and the associated relaxation time (T_1); then ω_2 = second crossover angular frequency and the associated relaxation time (T_2). T_1 and T_2 were calculated using the relation $T = 2\pi/\omega$.

loading may have a dominating effect, hence decreasing the relaxation time to a greater extent than the clay loading contributes to it. The presence of two crossover frequencies (the second being at low angular frequency) for the P(S-*co*-BA)–P-3.6% PCN, P(S-*co*-BA)–P-5% PCN and P(S-*co*-BA)–D-5% PCN show that for these nanocomposites there is long-range relaxation process taking place, which is caused by the presence of clay. This is to be expected since an increase in clay loading results in highly confined polymer chains; as such long-range relaxation processes take place over a longer period of time. Moreover, two crossover angular frequencies are an indication of the clay platelets having reached the percolation threshold [29]. A phenomenon where clay platelets will be touching each other i.e. a clay network. These results also indicate that the clay platelets were more thoroughly dispersed in the PCDBAB based nanocomposites relative to the DCTBAB as clay platelets formed a network at 3.6% clay loading for PCDBAB relative to 5% clay loading in the DCTBAB system.

The terminal gradients of both the PCDBAB and DCTBAB based nanocomposites decreased with an increase in clay loading, as reported by others [26,30,32]. The terminal gradients decreased from those typical of homopolymer behavior, i.e. $G^{I} \propto \sim \omega^2$ and $G^{II} \propto \omega^1$, to levels where the solid–liquid behavior dominates here $G^{I} > G^{II}$, at higher clay loadings, which is in agreement with literature [29]. The PDIs of the two series appeared to be important: the narrow PDI values of PCDBAB based nanocomposites resulted in better adherence to the expected relationships between G^{I} and G^{II} as a function of ω.

4. Conclusions

RAFT-mediated free-radical copolymerization of styrene and butyl acrylate was successfully achieved in miniemulsion using clay modified with either *N*-(4-((((dodecylthio)carbonothioyl)-thio)methyl)benzyl)-*N*,*N*-dimethylethanammonium (DCTBAB) or *N*,*N*-dimethyl-*N*-(4-(((phenylcarbonothioyl)thio)methyl)-benzyl)-ethanammonium (PCDBAB). The resulting stable lattices were P(S-*co*-BA)-PCNs with a morphology varying from semi-exfoliated to intercalated as the clay loading increased. The RAFT agents anchored onto clay, (i.e. DCTBAB and PCDBAB), resulted in polymers with molar masses and polydispersity indices that decreased as the clay loading increased. The control of the polymerization process increased with RAFT agent concentration. The melt rheological properties of PCNs were found to be dependent on molar mass, PDI, clay loading and clay morphology.

References

[1] Usuki A, Kojima Y, Kawasumi M, Okada A, Fukushima Y, Kurauchi T, et al. J Mater Res 1993;8:1179–84.
[2] Samakande A, Hartmann PC, Cloete V, Sanderson RD. Polymer 2007;48:1490–9.
[3] Okamoto M. Encyclopedia of nanoscience and nanotechnology. California: American Scientific Publishers; 2004.
[4] Rosorff M. Nano surface chemistry. New York and Basel: Marcel Dekker; 2002.
[5] Braunecker WA, Matyjaszewski K. Prog Polym Sci 2007;32. 93–146.
[6] Moad G, Rizzardo E, Thang SH. Aust J Chem 2006;59:669–92.
[7] Weimer MW, Chen H, Giannelis EP, Sogah DY. J Am Chem Soc 1999;121:1615–6.
[8] Di JB, Sogah DY. Macromolecules 2006;39:5052–7.
[9] Wheeler PA, Wang JZ, Baker J, Mathias LJ. Chem Mater 2005;17:3012–8.
[10] Wheeler PA, Wang JZ, Mathias LJ. Chem Mater 2006;18:3937–45.
[11] Yang YY, Lin JC, Yang WT, Jiang GJ. Polym Prepr 2003;44:855–6.
[12] Zhang B, Chen G, Pan C, Luan B, Hong C. J Appl Polym Sci 2006;102:1950–8.
[13] Di JB, Sogah DY. Macromolecules 2006;39:1020–8.
[14] Ding P, Zhang M, Gai J, Qu B. J Mater Chem 2007;17:1117–22.
[15] Zhang BQ, Pan CY, Hong CY, Luan B, Shi PJ. Macromol Rapid Commun 2006;27:97–102.
[16] Salem N, Shipp DA. Polymer 2005;46:8573–81.
[17] Moad G, Dean K, Edmond L, Kukaleva N, Li GX, Mayadunne RTA, et al. Macromol Symp 2006;233:170–9.
[18] Moad G, Li G, Pfaendner R, Postma A, Rizzardo E, Thang S, et al. ACS Symp Ser 2006;944:514–32.
[19] Moad G, Li G, Rizzardo E, Thang SH, Pfaendner R, Wermter H. Polym Prepr 2005;46:376.
[20] Samakande A, Sanderson RD, Hartmann PC. Synth Commun 2007;37:3861–72.
[21] Samakande A, Juodaityte JJ, Sanderson RD, Hartmann PC. Macromol Mater Eng 2008;293:428–37.
[22] Samakande A, Hartmann PC, Sanderson RD. J Polym Sci Part A Polym Chem 2008;46:7114–26.
[23] Fornes TD, Yoon PJ, Keskkula H, Paul DR. Polymer 2001;42:9929–40.
[24] Galgali G, Ramesh C, Lele A. Macromolecules 2001;34:852–8.
[25] Krishnamoorti R, Giannelis EP. Macromolecules 1997;30:4097–102.
[26] Okada K, Mitsunaga T, Nagase Y. Korea-Aust Rheol J 2003;15:43–50.
[27] Xu M, Choi YS, Kim YK, Wang KH, Chung IJ. Polymer 2003;44:6387–95.
[28] Ren JX, Silva AS, Krishnamoorti R. Macromolecules 2000;33:3739–46.
[29] Zhao J, Morgan AB, Harris JD. Polymer 2005;46:8641–60.
[30] Kim TH, Lim ST, Lee CH, Choi HJ, Jhon MS. J Appl Polym Sci 2003;87:2106–12.
[31] Lim ST, Lee CH, Choi HJ, Jhon MS. J Polym Sci Part B Polym Phys 2003;41:2052–61.
[32] Ma HY, Tong LF, Xu ZB, Fang ZP. Polym Degrad Stab 2007;92:1439–45.
[33] Moraes RP, Santos AM, Oliveira PC, Souza FCT, Amaral M, Valera TS, et al. Macromol Symp 2006;245–246:106–15.
[34] Solomon MJ, Almusallam AS, Seefeldt KF, Somwangthanaroj A, Varadan P. Macromolecules 2001;34:1864–72.
[35] Hartmann PC, Dieudonne P, Sanderson RD. J Colloid Interface Sci 2005;284:289–97.
[36] Feldermann A, Toy AA, Phan H, Stenzel MH, Davis TP, Barner-Kowollik C. Polymer 2004;45:3997–4007.
[37] Postma A, Davis TP, Li GX, Moad G, O'shea MS. Macromolecules 2006;39:5307–18.
[38] Perrier S, Takolpuckdee P. J Polym Sci Part A Polym Chem 2005;43:5347–93.
[39] Bowes A, Mcleary JB, Sanderson RD. J Polym Sci Part A Polym Chem 2007;45:588–604.
[40] Muthukrishnan S, Pan EH, Stenzel MH, Barner-Kowollik C, Davis TP, Lewis D, et al. Macromolecules 2007;40:2978–80.
[41] Zhao YL, Perrier S. Macromolecules 2006;39:8603–8.
[42] Gardebien F, BreDas J, Lazzaroni R. J Phys Chem B 2005;109:12287–96.
[43] Leigh ID, Mcdonald MP, Wood RM, Tiddy GJT, Travethan MA. J Chem Soc Faraday Trans 1 1981;77:2867–76.
[44] Leontidis E, Kyprianidou-Leodidou T, Caseri W, Robyr P, Krumeich F, Kyriacou KC. J Phys Chem B 2001;105:4133–44.
[45] Metivaud V, Lefevre A, Ventola L, Negrier P, Moreno E, Calvet T, et al. Chem Mater 2005;17:3302–10.
[46] Smith K, El-Hiti GA, Hammond MEW, Bahzad D, Li ZQ, Siquet C. J Chem Soc Perkin Trans 1 2000:2745–52.
[47] Luo J, Daniel IM. Compos Sci Technol 2003;63:1607–16.
[48] Fu X, Qutubuddin S. Polymer 2001;42:807–13.
[49] Tyan H, Wei K, Hsieh T. J Polym Sci Part B Polym Phys 2000;38:2873–8.
[50] Zhang W, Chen DZ, Zhao QB, Fang Y. Polymer 2003;44:7953–61.
[51] Noh MW, Lee DC. Polym Bull 1999;42:619–26.
[52] Yu Y, Yeh J, Liou S, Chang Y. Acta Mater 2004;52:475–86.
[53] Turi EA. Thermal characterization of polymeric materials. 2nd ed., vol. 1. San Diego: Academic Press; 1997.
[54] Meincke O, Hoffmann B, Dietrich C, Friedrich C. Macromol Chem Phys 2003;204:823–30.
[55] Chastek TT, Stein A, Macosko C. Polymer 2005;46:4431–9.